Hyperfine Interact (2009) 191:33–40
DOI 10.1007/s10751-009-9981-0

Exchange-spring magnets based on $L1_0$-FePt ordered phase

R. Ciprian · M. Carbucicchio · G. Turilli

Published online: 1 April 2009

Abstract Thin bi-layers constituted by a hard $L1_0$-FePt layer and a soft Fe layer were obtained using respectively an rf sputtering device and an UHV e-beam evaporation technique. Magneto-Optical Kerr Effect magnetometry, Atomic/Magnetic Force Microscopy and Conversion Electron Mössbauer Spectroscopy were used in order to correlate the magnetic properties of the bi-layers with the effects of the interdiffusion at the interfaces. It has been found that the evaporated Fe can easily diffuse into the hard film, giving raise to the formation of a region containing small particles of both Fe and Fe-rich FePt which show a superparamagnetic behaviour. The ferromagnetic Fe film can grow only on this region. The system shows (i) a preferred orientation of the easy magnetization axis along the direction normal to the film plane, and (ii) a single-phase magnetic behaviour due to the strong exchange coupling which established between the constituent phases.

Keywords $L1_0$-ordered FePt · Perpendicular magnetic anisotropy · Exchange-spring magnet · Interdiffusion phenomena · Mössbauer spectroscopy

1 Introduction

Nanostructured magnetic films and multilayers display peculiar properties which proved to be very interesting from both theoretical and technological point of view. In the field of micro-electromechanical systems (MEMS), permanent magnets and recording devices, particular attention is addressed to the development of systems constituted by exchange coupled soft and hard magnetic phases, showing a single

R. Ciprian (✉) · M. Carbucicchio
Department of Physics, University of Parma, Parma, Italy
e-mail: ciprian@fis.unipr.it

G. Turilli
IMEM Laboratory, CNR, Parma, Italy

phase magnetic behaviour [1, 2]. A considerable research activity has been addressed to investigate the structural and magnetic properties of nanocomposites where $L1_0$-ordered FePt film constitutes the hard phase. In effect, FePt alloy synthesized at high temperature shows a fct structure ($L1_0$) with strong uniaxial magnetocrystalline anisotropy along the contracted *c*-axis. The epitaxial growth of the system with the *c*-axis oriented along the normal to the film plane can induce a perpendicular easy magnetization axis [3–6].

In the present work, magnetic planar nanocomposites were grown in the form of bi-layers showing a strong perpendicular magnetocrystalline anisotropy. The hard phase was constituted by a $L1_0$-ordered FePt film and the soft phase by a Fe layer. The FePt hard films were deposited by rf sputtering on MgO (100) monocrystalline substrates with and without a Pt underlayer 20 nm thick. The soft films in turn were deposited using an UHV e-beam evaporation technique, assuming that it can favour a good arrangement of iron atoms, low stresses at the interfaces and therefore the establishing of a strong exchange coupling between the magnetic phases. The use of two different techniques properly selected for growing each component of the bi-layers represents an innovative approach, suitable for positive developments in the field of the exchange-spring magnets.

Previous works on model systems [7–9] pointed out that a determining role in the exchange coupling between different magnetic layers is played by their nature and morphology, and by the interdiffusion phenomena occurring at the interfaces. In order to analyse these effects, Mössbauer spectroscopy has been performed on FePt/Fe bi-layers and related to the exchange coupling occurring between the soft and hard phases.

2 Experimental procedure

$Fe_{52}Pt_{48}$ films, 15 and 20 nm thick, were deposited by rf sputtering onto MgO (100) single crystal substrates by alternating Fe and Pt thin layers, adjusting the relative thickness in order to obtain the desired FePt composition. The growth rates were 12.7 and 11.7 Å/min, respectively, and the substrate temperature was 550°C. In order to reduce the lattice mismatch between film and substrate, a 20 nm thick underlayer of Pt was grown onto a previously deposited 1 nm thick seed layer of Fe, which favours the epitaxial growth of Pt at low temperature [10]. These films were finally selected as the hard components for building exchange-coupled hard/soft bi-layers. The soft component was a 7 nm thick layer of ^{57}Fe e-beam evaporated at room temperature in ultra-high vacuum. The growth rate of these outer layers was ∼6 Å/min and a vacuum $\sim 10^{-9}$ mbar. The layer thickness was measured "in situ" by a quartz micro-balance.

Conversion Electron Mössbauer Spectroscopy (CEMS) measurements were carried out without breaking the vacuum, using a 55 mCi ^{57}Co(Rh) source. A least squares minimization routine with a combination of linear and non linear regressions was used to fit the spectra as a superposition of Lorentzian lines. The isomer shifts IS are referred to α-Fe. Considering that the hard film is thin and contains natural iron, CEMS measurements are in practice concerning only the soft film and the ^{57}Fe-containing compounds eventually formed at the soft/hard interface. The

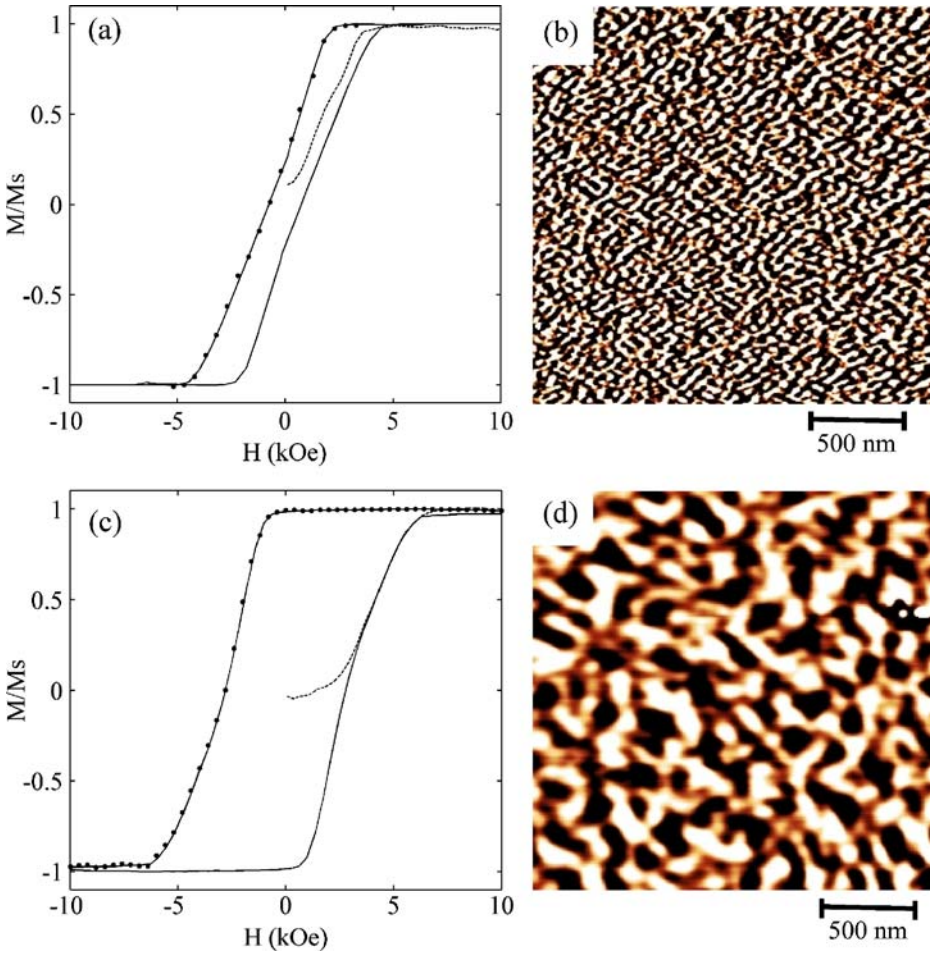

Fig. 1 **a** and **c** MOKE measurements (— hysteresis loop, --- initial magnetization curve, ••• remanence curve), and **b** and **d** MFM images for FePt(20 nm) and Pt/FePt(20 nm) films respectively

morphology and the domain patterns were analyzed by UHV Atomic and Magnetic Force Microscopy (AFM/MFM) in tapping mode, without breaking the vacuum, using cantilevers with non-magnetic and CoCr-coated magnetic tips, respectively. For the magnetic image, the lift distance was 50 nm. The magnetic properties of the samples were measured using a Magneto-Optical Kerr Effect (MOKE) magnetometer in polar geometry, with *s*-polarized 633 nm He–Ne laser light. The DCD demagnetization curves were acquired starting from the samples saturated in the positive field direction and applying a negative magnetic field of increasing intensity. XRD measurements performed on hard FePt films indicates a good epitaxial growth of the film with the presence of only the fundamental (002) and superstructure (001) reflections of the $L1_0$-FePt phase.

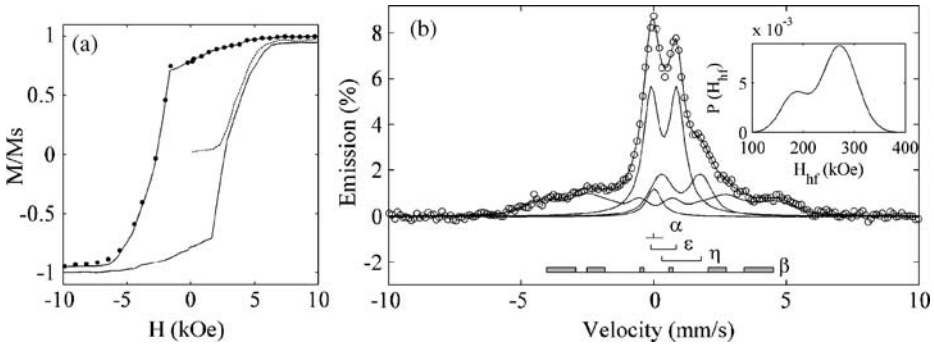

Fig. 2 **a** MOKE measurements (— hysteresis loop, --- initial magnetization curve, ••• remanence curve) and **b** CEMS spectrum and the hyperfine magnetic field distribution corresponding to β contribution for Pt/FePt(20 nm)/^{57}Fe system

Table 1 Mössbauer parameters of the contributions to the spectra reported in Figs. 2(b) and 5

	α	α_1	ε	β	β_I	η^b
IS(mm/s)	0.01	–	0.38	0.24	0.11	0.99
ΔE_Q(mm/s)	–	–	1.10	0.18	0.18	1.41
H_{hf} (kOe)	–	329.8	–	283, 194[a]	290, 243[a]	–

[a] H_{hf} values corresponding to the main peaks of the hyperfine field distribution
[b] Attributable to ^{57}Fe atoms which entered the MgO substrate [11] during the e-beam evaporation in zones which remained shielded by the substrate locking system during the FePt sputtering deposition

3 Results and discussion

Figure 1 shows the MOKE and MFM measurements performed for the FePt film 20 nm thick [FePt(20 nm), Figs. 1(a) and (b)] and for FePt film 20 nm thick grown on the Pt underlayer [Pt/FePt(20 nm), Figs. 1(c) and (d)].

For both films the initial magnetization curves show a kink closed to the coercive field H_c, suggesting that the predominant coercivity mechanism is the domain wall pinning. The quite complete superposition between the loops and the remanence curves unambiguously testifies the very high hardness of the films.

The presence of the Pt underlayer gives rise to (a) a strong increase of the coercivity inducing defects in the alloy, which act as pinning sites for the domain wall motion, and (b) a strong enhancement of the loop squareness, indicating a better alignment of the *c*-axis along the direction perpendicular to the film plane. The higher anisotropy changes the domain shape from a stripe- [Fig. 1(b)] to a maze-like pattern [Fig. 1(d)], and induces a relevant increase of the domain sizes.

Figure 2(a) shows the magnetic measurements performed for the hard Pt/FePt(20 nm) film covered by a 7 nm thick soft layer of ^{57}Fe [Pt/FePt(20 nm)/^{57}Fe]. The recoil loops indicate only irreversible rotations of the magnetization and therefore, a behaviour typical of an exchange-spring magnet. The presence of the soft layer gives rise to a reduction of the remanence ratio M_r/M_s, substantially without decreasing the value of the coercive field.

The CEMS spectrum performed on the same film is reported in Fig. 2(b) and the relative hyperfine parameters summarized in Table 1. Unexpectedly, no contribution

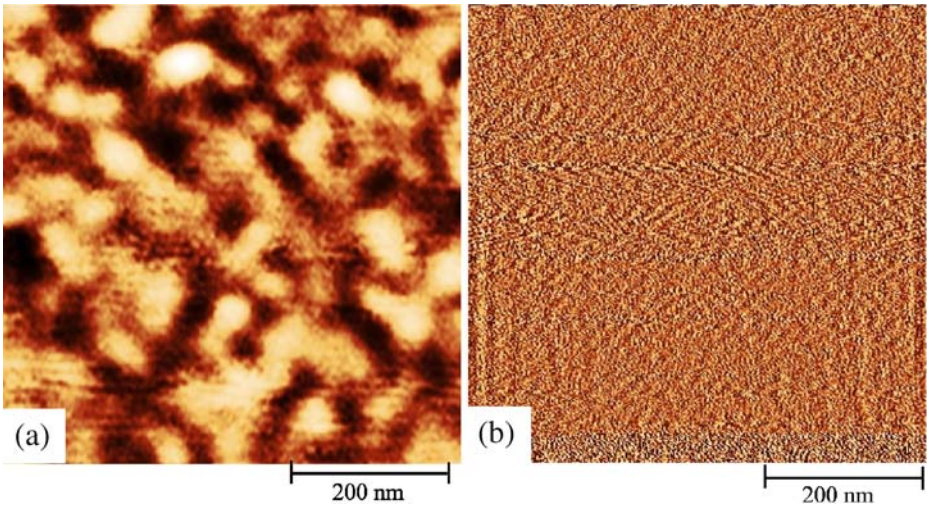

Fig. 3 AFM images for **a** Pt/FePt(20 nm) and **b** Pt/FePt(15 nm) films

Table 2 Remanence ratio $M_r\,(\perp)/M_s$, squareness S_q and Coercive field H_c of analysed samples

Analyzed samples	$M_r\,(\perp)/M_s$(%)	S_q(%)	H_c(kOe)
FePt(20)	23	50	0.75
Pt/FePt(20)	99	67	3.00
Pt/FePt(20)/^{57}Fe	77	76	2.86
Pt/FePt(15)	100	88	3.40
Pt/FePt(15)/^{57}Fe	100	80	2.40

from ferromagnetic iron is present in the Mössbauer spectrum. A possible explanation is that the evaporated ^{57}Fe diffuses within the surface regions of the underlying hard film along preferential paths such as grain boundaries and, subsequently, (a) coalesces in low density zones giving raise to small particles of iron showing a superparamagnetic behaviour (single line α), and (b) reacts with FePt giving raise to ^{57}Fe-rich FePt compounds with a large grain size distribution showing collapsing hyperfine magnetic fields (β contribution) up to the superparamagnetic limit (ε doublet).

These large diffusion phenomena suggest that the hard Pt/FePt(20 nm) film is characterized by a very low compactness. In agreement, the AFM image of the uncovered Pt/FePt(20 nm) film [Fig. 3(a)] shows a surface with a very granular and roughness morphology.

A different situation occurs in the case of the rf sputtered film 15 nm thick [Pt/FePt(15 nm)]. In this case, the surface morphology is much more compact [Fig. 3(b)] reasonably because of the reduced thickness of the hard film which favours the establishing, during the deposition stage, of a lower temperature gradient between the substrate and the film surface. The MOKE measurements [Fig. 4(a)] show that the reduction of the thickness induces a considerable increase in both coercive field and loop squareness S_q (Table 2).

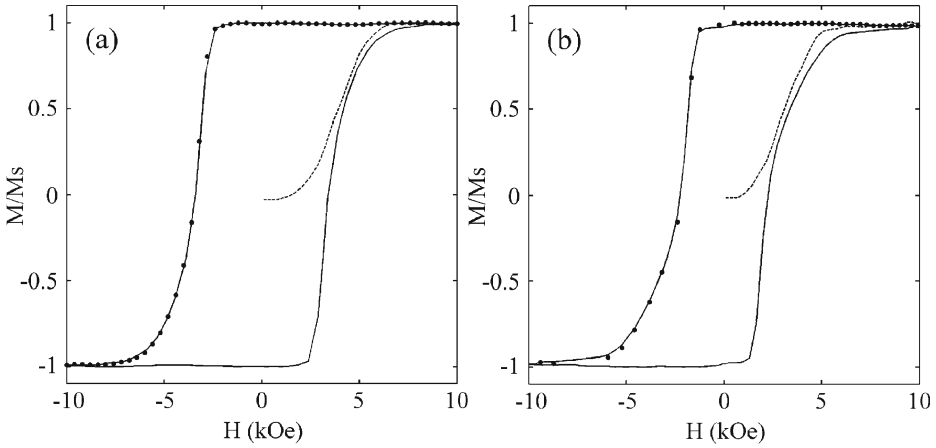

Fig. 4 MOKE measurements for **a** Pt/FePt(15 nm) and **b** Pt/FePt(15 nm)/^{57}Fe samples: (—) hysteresis loop, (---) initial magnetization curve, (•••) remanence curve

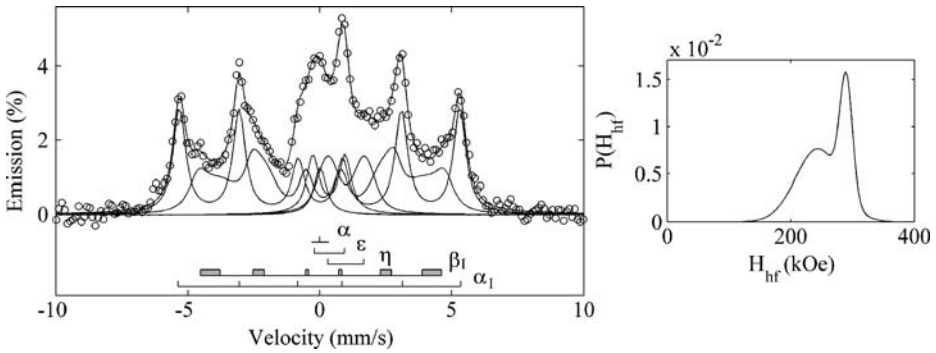

Fig. 5 CEMS spectrum for sample Pt/FePt(15 nm)/^{57}Fe and the hyperfine magnetic field distribution corresponding to β_1 contribution

Figure 4(b) shows the MOKE measurements recorded for the Pt/FePt(15 nm) film covered by 7 nm of ^{57}Fe [Pt/FePt(15 nm)/^{57}Fe]. The Fe deposition caused a decrease in the coercive field from 3.4 kOe to 2.4 kOe while the remanence ratio remained unchanged: $M_r\,(\perp)\big/M_s = 1$. The single phase magnetic behaviour is deduced by the shape of the hysteresis loop and by its complete overlapping with the remanence curve.

The considerable differences observed between the magnetic properties of the Pt/FePt(15 nm)/^{57}Fe and Pt/FePt(20 nm)/^{57}Fe bi-layers can be ascribed to the different surface morphology and defectiveness of the hard phases (Fig. 3) which may well influence anisotropy and coercivity mechanisms, as well as the interdiffusion phenomena.

The CEMS spectrum recorded for Pt/FePt(15 nm)/^{57}Fe is shown in Fig. 5 and the corresponding hyperfine parameters are reported in Table 1.

From the comparison between the spectra measured for Pt/FePt(20 nm)/^{57}Fe and Pt/FePt(15 nm)/^{57}Fe bi-layers [Figs. 2(b) and 5] it follows that:

1. $\alpha-$iron, which in sample Pt/FePt(20 nm)/^{57}Fe is only present in the form of small particles, in Pt/FePt(15 nm)/^{57}Fe is present both as small particles (singlet α) and as a normal ferromagnetic phase (sextet α_1), the last giving the prevailing contribution to the spectrum.
2. The contribution from ^{57}Fe-rich FePt superparamagnetic small particles (ε doublet) is considerably decreased in the spectrum of Pt/FePt(15 nm)/^{57}Fe.

The H_{hf} distribution for ^{57}Fe-rich FePt compound in Pt/FePt(15 nm)/^{57}Fe shows peaks which are better defined than that in Pt/FePt(20 nm)/^{57}Fe and shifted towards higher values. These facts suggest that this compound is present in Pt/FePt(15 nm)/^{57}Fe with a better defined stoichiometry and with a narrower particle size distribution.

4 Conclusions

$L1_0$-ordered FePt films showing a perpendicular anisotropy have been epitaxially grown on MgO single crystals by rf sputtering. This technique favours the formation of pinning sites which hinder the domain wall motion and, therefore, considerably promote the high coercivity of the film.

The presence of a Pt underlayer determines an increase of the magnetic hardness and favours the epitaxial growth with the development of a strong perpendicular anisotropy. The reduction of the film thickness causes a further improvement of the anisotropy and of the loop squareness.

The e-beam evaporation of a soft layer of iron on the top of the hard films gives rise to bi-layered systems showing a single phase magnetic behaviour. The soft layer is constituted either by Fe-rich FePt or by ferromagnetic Fe and Fe-rich FePt, depending on the surface morphology and compactness of the hard film. In both cases the interface is a very thin layer constituted by FePt and iron both in the form of small particles.

References

1. Kneller, E.F., Hawig, R.H.: The exchange-spring magnet: a new material principle for permanent magnets. IEEE Trans. Magn. **27**, 3588–3600 (1991)
2. Coey, J.M.D., Skomski, R.: New magnets from interstitial intermetallics. Phys. Scr. **T49**, 315–321 (1993)
3. Barmak, K., Kim, J., Shell, S., Svedberg, E.B., Howard, J.K.: Calorimetric studies of the A1 to $L1_0$ transformation in FePt and CoPt thin films. Appl. Phys. Lett. **80**, 4268–4270 (2002)
4. Spada, F.E., Parker, F.T., Platt, C.L., Howard, J.K.: X-ray diffraction and Mössbauer studies of structural changes and $L1_0$ ordering kinetics during annealing of polycrystalline $Fe_{51}Pt_{49}$ thin films. J. Appl. Phys. **94**, 5123–5134 (2003)
5. Endo, Y., Kikuchi, N., Kitakami, O., Shimada, Y.: Lowering of ordering temperature for fct Fe–Pt in Fe/Pt multilayers. J. Appl. Phys. **89**, 7065–7067 (2001)
6. Takahashi, Y.K., Hono, K., Shima, T., Takanashi, K.: Microstructure and magnetic properties of FePt thin films epitaxially grown on MgO (001) substrates. J. Magn. Magn. Mater. **267**, 248–255 (2003)

7. Carbucicchio, M., Grazzi, C., Lanotte, L., Rateo, M., Ruggiero, G., Turilli, G.: Co/Fe Multilayers as Planar Magnetic Nanocomposites. Hyperfine Interact. **139–140**, 553–559 (2002)
8. Carbucicchio, M., Bennett, S., Berry, F.J., Prezioso, M., Rateo, M., Turilli, G.: Structural order and magnetic anisotropy transition in Co/Fe multilayers. J. Appl. Phys. **93**, 7631–7633 (2003)
9. Agazzi, L., Bennett, S., Berry, F.J., Carbucicchio, M., Rateo, M., Ruggiero, G., Turilli, G.: Magnetic interactions and interface properties in Co/Fe multilayers. J. Appl. Phys. **92**, 3231–3234 (2002)
10. Lairson, B.M., Visokay, M.R., Sinclair, R., Hagstrom, S., Clemens, B.M.: Epitaxial Pt(001), Pt(110), and Pt(111) films on MgO(001), MgO(110), MgO(111), and Al_2O_3(0001). Appl. Phys. Lett. **61**, 1390–1392 (1992)
11. Potzger, K., Reuther, H., Zhou, S., Mücklich, A., Grötzschel, R., Eichhorn, F., Liedke, M.O., Fassbender, J., Lichte, H., Lenk, A.: Ion beam synthesis of Fe nanoparticles in MgO and yttria-stabilized zirconia. J. Appl. Phys. **99**, 08N701–3 (2006)